Journal of Ambient Intelligence and Humanized Computing (2020) 11:2027–2040
https://doi.org/10.1007/s12652-019-01212-6

ORIGINAL RESEARCH

An intelligent flying system for automatic detection of faults in photovoltaic plants

Vincenzo Carletti[1] · Antonio Greco[1] · Alessia Saggese[1] · Mario Vento[1]

Received: 7 October 2018 / Accepted: 14 January 2019 / Published online: 21 January 2019

Abstract
For several years, fault diagnosis of photovoltaic (PV) plants has been manually performed by the human operator by a visual inspection or automatically, by evaluating electrical measures collected by sensors mounted on each PV module. In recent years, a notable interest of the scientific community has been devoted towards the definition of algorithms able to automatically analyse the sequence of images acquired by a thermal camera mounted on board of an unmanned aerial vehicle (UAV) for early PV anomaly detection. In this paper, we define a model-based approach for the detection of the panels, which uses the structural regularity of the PV string and a novel technique for local hot spot detection, based on the use of a fast and effective algorithm for finding local maxima in the PV panel region. Finally, we introduce the concept of global hot spot detection, namely a multi-frame recognition of PV faults which further improves the anomaly detection accuracy of the proposed method. The algorithm has been designed and optimized so as to run in real-time directly on an embedded system on board of the UAV. The accuracy of the proposed approach has been experimented on several video sequences with a standard protocol in terms of Precision, Recall and F-Score, so that our dataset and our quantitative results can be used for future comparisons and to evaluate the reliability of computer vision techniques designed for thermographic PV inspection.

1 Introduction

In the last 15 years we have assisted to an exponential growth of renewable energy produced with solar photovoltaic (PV) plants. Studies conducted by Solar Power Europe, the new European Photovoltaic Industry Association, report that in 2016 the electricity produced by PV panels has been about 300 GW, while the projected capacity for 2018 is around 500 GW, with an impressive increase of about 100 GW per year.[1] Once a PV system is installed, it is important to monitor its energy efficiency, since the choice to use such a plant is not only an investment on an eco-sustainable technology, but, above all, a source of long-term profit. In this scenario, the PV plant monitoring plays a crucial role, offering the possibility to retrieve information about possible loss of power of the PV modules, and also to solve the faults immediately and then to prevent increasing efficiency drops.

1.1 PV faults taxonomy

The need of monitoring such plants determined, in the last decade, a broad analysis on the types of PV faults that can occur during the operational lifetime of a PV plant, as evident in Grimaccia et al. (2017a), Tsanakas et al. (2016) and Djordjevic et al. (2014). Tsanakas et al. (2016) attribute most of the faults to optical degradation and electrical mismatches. Djordjevic et al. (2014) report discolouration, caused by low encapsulant quality or long exposition to high temperature and humidity, and oxidation or corrosion, mainly due to loss of adhesion and delamination, as examples of optical faults which reduce the sunlight absorbed by the solar cells [about 25% of the PV faults are due to optical degradation (Grimaccia et al. 2017a)]. Almost all the other PV anomalies are electrical mismatches due to different aging phenomena. For example, poor soldering

✉ Alessia Saggese
asaggese@unisa.it

Vincenzo Carletti
vcarletti@unisa.it

Antonio Greco
agreco@unisa.it

Mario Vento
mvento@unisa.it

[1] Department of Information and Electrical Engineering and Applied Mathematics, University of Salerno, Fisciano, Italy

[1] http://www.solarpowereurope.org.

or mechanical and thermal stress can produce cell cracks (Djordjevic et al. 2014) of variable entities. Snail trails (or tracks), which consists of discolouration of the silver grid across the cell or along the edge (Djordjevic et al. 2014) and represent more than 20% of the PV anomalies (Grimaccia et al. 2017a), are typically detected in presence of invisible cell cracks (Tsanakas et al. 2016). Another significant percentage of faults, around 10% (Grimaccia et al. 2017a), is due to defective by-pass diodes or disconnections (Tsanakas et al. 2016). The remaining PV anomalies described in Grimaccia et al. (2017a) and Tsanakas et al. (2016) are typically related to environmental factors, such as shading, dirt or dust retention and physical impacts.

1.2 PV anomaly detection techniques

The classical way for detecting PV anomalies is the visual inspection of the panels and some electrical parameters measurement on each module (Quater et al. 2014). In the first case, one or more experts are required to visually detect alterations of the appearance of the panels, denoting the presence of faults. In the second case, many electrical sensors are installed on the PV modules to measure the energy efficiency of the plant. Such inspection techniques are complementary, since electrical measures can detect the effects of the faults (loss of energy efficiency), while visual inspections can identify the causes of the anomalies (shadows, cracks, trees, leaves and so on). In both the cases, these approaches are acceptable for small PV plants, while become very expensive for large PV array fields.

Indeed, the time and the money required for the classic inspections increase proportionally with the PV system size. For this reason, there is a growing interest for alternative and cost-efficient methods for automatically monitoring large PV plants. A very efficient and effective solution is the thermographic analysis, which detects anomalies by using images captured with thermal cameras. Hot spots are very frequent anomalies observed on PV panels during their operational lifetime and consist of heating effects due to the presence of a solar cell which generates electrical current smaller than the string electrical current of the module (Tsanakas et al. 2016). Since this effect can be observed in correspondence of most of the above mentioned PV anomalies (optical degradation, electrical mismatches, shading, physical impacts, dust), the detection of hot spots on PV panels can be considered a valid method for PV faults monitoring.

1.3 Thermographic inspections with UAVs

The effectiveness of thermographic analysis has been tested in several preliminary laboratory experiments performed in Buerhop et al. (2012a, b), Buerhop and Scheuerpflug (2014) and Hu et al. (2014a, b). The encouraging results focused the attention of the researchers on the possibility to use such inspection technique for large PV plants. The solution found by the experts of this field, which is become a standard de facto in the last years, is the use of special purpose unmanned aerial vehicles (UAVs), as drones, equipped with a thermal camera for faults detection. Such a method has two main advantages: (1) it is suited for large PV array fields inspection, since the whole plant can be explored in a few flights (depending on the size of the plant and the UAV's battery life); (2) the cost and time required for the analysis are significantly pulled down with respect to the classical inspection techniques. The suitability of the solution (Aghaei et al. 2014) has been evaluated with qualitative analysis performed on real PV array fields in Grimaccia et al. (2017a), Tsanakas et al. (2016) and Djordjevic et al. (2014) to verify which anomalies are visible with moving cameras, in Leva et al. (2015), Grimaccia et al. (2015) and Aghaei et al. (2016a) to identify the impact of the flight parameters on the detection capabilities and in Quater et al. (2014) and Grimaccia et al. (2017b) to test the reliability of special purpose UAVs.

In particular, two typologies of architectures for thermographic anomalies detection can be identified: (1) the plant images are analysed in real-time during the UAV flight; (2) the image analysis is performed off-line, by analysing the video recorded during the inspection. Of course, the first solution is faster and allows the pilot to verify in real-time if the PV modules have been correctly inspected, but it requires a careful software design to speed up the image processing algorithm.

The UAV typically carries not only a thermal camera, but also a visible light camera. The former is used for the thermographic analysis, since it is more suitable for detecting faults; viceversa, the latter can be useful for retaining coloured images associated to a possible anomaly recognized by the image processing algorithm. The idea is that images of the defective PV modules, accompanied by the geographic coordinates measured by the GPS sensor, can represent a very powerful and effective instrument for automatic PV inspection (Tsanakas et al. 2017). However, the current precision of GPS sensors is in the order of a few metres, while the accuracy required for PV panels geo-localization should be at most a few centimetres. Therefore, at the current state of technology, the computer vision algorithm can not exploit the geographical coordinates estimated by the GPS sensors to recognize and identify each PV panel, but should provide a mechanism to track each module and detect possible anomalies in the image.

1.4 Related works and contributions

In this section, we analyse the computer vision part of the architecture, which has not received in the literature the

attention it would deserve. Furthermore, we highlight the contributions with respect to methodologies available in the literature. The automatic detection of PV modules and the recognition of faulty panels with image processing techniques is completely different and significantly more challenging than the PV thermographic analysis performed in controlled laboratory conditions. The state of the art papers in this field point out the great economic advantage which derives from the use of this architecture, showing the feasibility and the suitability of the PV inspection with UAVs and thermal cameras only from a qualitative point of view. However, it is not sufficient to demonstrate that PV fault diagnosis can be carried out, but it is even more important to evaluate its effectiveness with quantitative performance indices. In fact, the real economic advantage is obtained only if the computer vision algorithm is really able to detect PV modules and their anomalies with sufficient accuracy.

To this aim, we analyse and address the problem considering three different crucial aspects for the first time in literature: panel detection, local hot spot detection and global hot spot detection.

1.4.1 PV panel detection

PV panel detection is the capability of the computer vision algorithm to distinguish PV modules from any other object in the image. It is the preliminary step necessary for the selection of the area covered by the PV plant and the identification of each individual panel, delimiting its area with a bounding box. Such operation is very challenging, due to the vibrations of the UAV which generates blurred images and to the thermal irregularities that can produce images so noisy that the contrast between adjacent PV modules becomes practically absent. Furthermore, the PV modules in a plant are all equals, so it is not possible to use information such as color, shape and texture for detection, but only structural features (typical grid shape) that are not easy to identify in presence of noisy images. Finally, it can not be neglected that if the drone flies at variable altitudes or the panels of the plant have different inclinations, the size of the module in the image plane may change, so making the detection even more difficult.

The authors of most of the scientific methods proposed in this field typically do not consider the problem of panel detection separately from the other steps; consequently, most of them neglect the above mentioned difficulties and do not give a detailed description of the solutions designed for dealing with them. Aghaei et al. (2016b) propose an image mosaicing technique for a richer description of the PV plant by merging many thermal images and counting the total number of PV modules; however, the authors describe the way to identify panel strings and defect areas, without giving details about the procedure for single modules detection. Addabbo et al. (2017) use a template matching technique and a normalized cross correlation as similarity measure to detect panels in large PV array fields; nevertheless, no information about the training of the system is provided. Guerriero and Daliento (2017) detect the border of the panels in thermal images by extracting those points whose temperature is lower than the median value of the temperature distribution; as already mentioned, such choice is not robust when the contrast between adjacent panels is low and, in any case, does not consider that panel junctions can be very hot. Dotenco et al. (2016) carry out panel detection by using a Gaussian Mixture Model (GMM) for PV modules segmentation and extract single panels regions after a normalization in terms of luminance, orientation and size of each module; the authors fix temperature and color thresholds for normalization, so making the method probably not easily adaptable to different scenarios. Grimaccia et al. (2017b) apply color filtering on classic visual images to obtain a mosaic representation of the plant used to recognize and number all the panels; the drawback of this solution is the usage of two different cameras, one classic and one thermal, for panel detection and fault diagnosis.

Contribution 1 Differently from state of the art methodologies, we introduce a model based approach for panel detection, aimed at exploiting the grid-based structure of the plant instead than traditionally employed color-based information. The main advantage of avoiding color information for panel detection is that the algorithm does not require the definition of static luminance thresholds. In more details, we perform a preprocessing of the image, aimed at enhancing the contrast between adjacent PV modules; such preliminary operation makes the algorithm robust to various weather conditions, thermal image irregularities and UAV vibrations.

1.4.2 Local hot spot detection

Most of the PV faults appear on the thermal image as hot spots, so anomalies and hot spots are interchangeable terms from the image analysis point of view. The term local means that the detection is performed only on the current frame, without considering the history of the hot spot in the video sequence. Hot spot detection is typically performed only in the PV module area, delimited by the bounding box determined during panel detection step, searching for regions with luminance (temperature) higher than a threshold or with respect to the average. Although the task may be considered easy when the panel detection is accurate, a local hot spot detection algorithm must deal with two types of problems. The first occurs in particular weather conditions or in certain moments of the day, when the luminance difference between the hot spot and the rest of the PV module is almost imperceptible; such condition makes it hard to define a threshold for color-based hot spot detection techniques.

The second problem is related to the junctions of the PV panels, which are typically characterized by a higher temperature and, thus, completely indistinguishable from hot spots, except for the position they occupy in the module. The way to avoid such kind of false positives is the exclusion of the borders from the elaboration. Of course, the mistakes made during this step are strictly dependent on the panel detection error, since a bounding box not precisely centred on the PV module may cause the wrong exclusion of a hot spot or the wrong classification of a panel junction as hot spot.

State of the art methods do not take into account the problem of hot panel junctions and typically apply color-based heuristics for recognizing faulty PV modules. For example, Tsanakas et al. (2015) apply Canny edge detection on thermal images, without preliminary PV panel segmentation, to identify luminance variations and discontinuities due to the higher temperature of hot spots with respect to the normal operating temperature. Jiang et al. (2016) propose a method based on curve fitting of gray histograms to detect hot spots. Grimaccia et al. (2017b) compute the average luminance of the panels, detected on visual images, to compute color thresholds used for detecting hot spots. Aghaei et al. (2015a) use Gaussian filter and a Laplacian model to detect possible defects and failure characteristics on the PV modules. The authors use a color threshold to determine the "hot area" of a panel and raise an alarm if the percentage of degradation (the ratio between hot area and the total area of the module) is greater than a certain value. The critical issue of this method is that the degradation threshold can not be the same for all the panels, since the hot spot may have various sizes. Such aspect has been faced in the paper (Aghaei et al. 2015b), where the authors provide more accurate heuristics for distinguishing hot areas in single modules. Dotenco et al. (2016) apply four feature sets, extracted on the PV panel region, to detect anomalies in PV modules: module medians, grid cell medians, histogram skewness and vertical projections. Arenella et al. (2017) use the Sobel edge detector to compute the gradient in each panel and select all the connected components with a luminance greater than a fixed threshold and that are not close to the borders. Considering that all these methods are based on color features and absolute static thresholds, they have problems when the contrast between hot spots and panel background is low or different with respect to the fixed threshold.

Contribution 2 Differently from available methods, we observe that from a thermographic point of view, a hot spot is a region of the PV panel characterized by a temperature, namely a luminance intensity, greater than the rest of the module. Thus, instead than using color based information, we formulate the hot spot detection problem in terms of local maxima searching in the image region delimited by the borders of the PV module. On this basis, the proposed approach uses the water filling, a fast and effective algorithm for finding local minima on depth images (Zhang et al. 2012); we adapted such algorithm for the purpose of local maxima search on thermal images. This is the first time that the problem of thermal anomaly detection on PV panels is formulated and addressed with a local maxima search algorithm.

1.4.3 Global hot spot detection

The overall accuracy of an automatic PV inspection system can be further improved introducing the concept of global hot spot detection, that is the capability of the computer vision algorithm to properly report, at the end of the passage on a specific PV module, the presence or the absence of a fault on that panel. The term global means that the detection accuracy is evaluated over all the frames where the PV panel is present, so that the same anomaly in different frames must be counted only once by the algorithm. Global hot spot detection is very challenging, since it requires the use of a tracking algorithm for uniquely identifying a PV panel in different frames. Objects tracking is typically faced by combining information about the position with some appearance features, encoding color, texture or shape, as shown in Yilmaz et al. (2006), Carletti et al. (2018) and Li et al. (2013). Anyway, in this scenario, the above features are not able to provide any contribution for discriminating a PV module from another one, being very similar each other from the appearance point of view. Consequently, only the position of the PV module in the image can be used as a discriminant feature for computing a similarity measure.

Contribution 3 To the best of our knowledge, this is the first time that the problem of global hot spot detection is defined and addressed in the literature, allowing us to achieve a significant improvement with respect to the local hot spot detection.

1.4.4 Performance evaluation and time processing analysis

Contribution 4 Another important contribution pertains the definition of a standard experimental protocol for the quantitative performance evaluation of PV inspection techniques, based on the well known computer vision accuracy indices of Precision, Recall and F-Score (Goutte and Gaussier 2005). Since the possible real scenarios are very variegate, we have used a wide dataset for our experiments, which consists of 15 videos acquired in real large PV plants. We produced for all the videos the ground truths for local and global hot spot detection, while the annotations for panel detection are available for a subset of 5 videos. Thanks to this exhausting work, the dataset provides annotations for 14,215 PV panels and 76 real hot spots visible 3654 times in the images. To the best of our knowledge it is far apart the wider dataset ever used in the literature [(Addabbo et al. (2017) use 270 frames, while

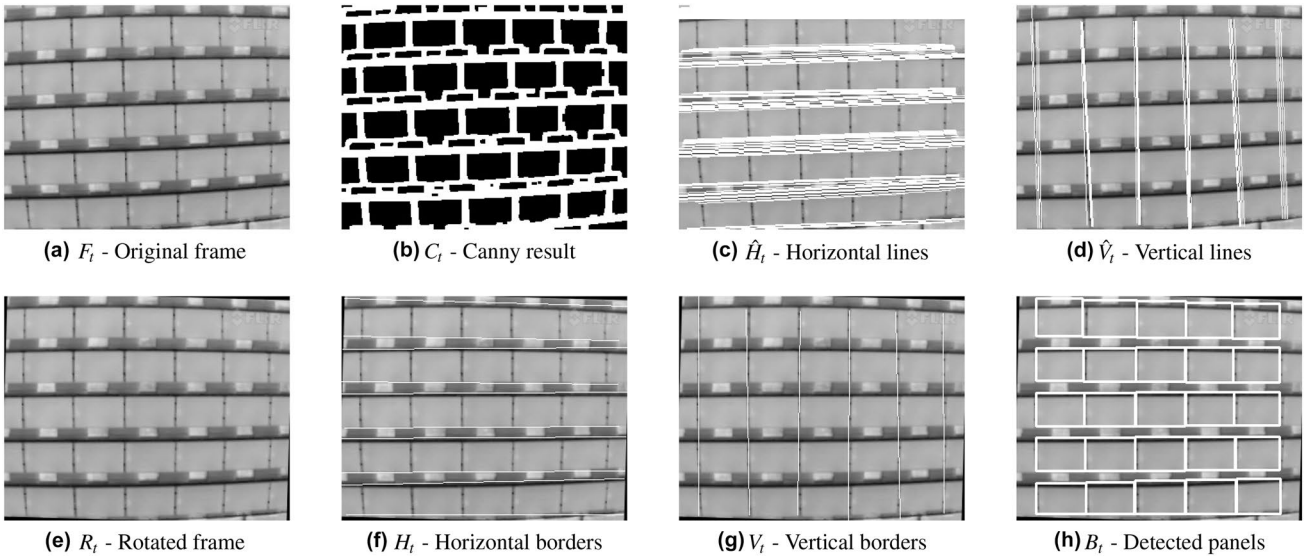

Fig. 1 **a** F_t: original frame captured by the thermal camera at time t; **b** C_t: binary image obtained after the application of Gaussian blur, Canny algorithm and morphological closure; **c** $\hat{H}_t$: horizontal lines detected after the application of Hough transform and horizontal line selection; **d** $\hat{V}_t$: vertical lines detected after the application of Hough transform and vertical line selection; **e** R_t: original frame rotated for simplifying grid detection; **f** H_t: horizontal borders of the panels detected with horizontal lines clustering; **g** V_t: vertical borders of the panels detected with vertical lines clustering; **h** P_t: panels detected at time t, surrounded by the corresponding bounding boxes B_t

Dotenco et al. (2016) only 61 images] and it is surely the only one with annotations for panels and hot spot detection.

Contribution 5 Another important aspect not yet considered in the literature is the evaluation of the time processing required by the proposed algorithms. As discussed above, the possibility to perform the image analysis during the flight has the following main advantages: the UAV pilot can receive a visual feedback directly during the flight; it implies that he can dynamically adapt the altitude, the speed and the direction of the flight in case some more information needs to be provided about a single PV module. It is important to note that in absence of a real time procedure, it could become necessary a second flight: for instance, in case of wind some frames could be affected by the blurring and some PV modules could be not visible by the camera, causing that the analysis could be not accurate enough. This implies a second notable advantage, namely a strongly time (and then cost) saving due to the introduction of a real-time fault detection system. In this paper we do not only analyse the time required by each step of the proposed algorithm, but also demonstrate that the method is able to process images in real-time on a mini-PC that can be easily equipped by the UAV during the flight.

2 Proposed method

In this section we will detail the proposed approach: in particular, PV panel detection in Sect. 2.1, local hot spot detection in Sect. 2.2 and finally global hot spot detection in Sect. 2.3.

2.1 PV panel detection

In order to deal with the problems mentioned in Sect. 1.4.1, we introduce a new pre-processing chain of the original frame F_t based on the following steps: Gaussian blur is first applied so as to remove thermal noise from the original image; the borders of PV modules are identified by means of the Canny algorithm; in order to further enhance the contrast between adjacent panels, we apply a morphological closure operation which is able to remove the residual noise and to thicken the borders of the PV modules. The main advantage of such approach is that no static color thresholds are needed, since the Canny

algorithm evaluates the luminance gradient for detecting contours. The resulting binary mask C_t, shown in Fig. 1b, is a coarse representation of the PV plant grid structure. We can note that the borders of adjacent panels can be now clearly visualised.

To detect separately each PV module, we propose a finer model-based representation of the panel using the Hough transform, which allows us to detect all the lines $L_t = (l_t^1, ..., l_t^{|L|})$, where $|L|$ is the number of lines detected at time t on C_t. Note that, differently from our previous work (Arenella et al. 2017), the Hough transform is applied on the image C_t instead than on the original frame F_t. In Sect. 3 we demonstrate that such difference is not negligible, since our proposed pre-processing steps allow to significantly improve the performance thanks to the contrast enhancement between adjacent modules.

Unfortunately, the application of the Hough transform is not sufficient to determine the grid structure of the PV plant, since the set L_t contains: (1) several spurious lines; (2) more than one line for each panel junction; (3) various lines that are smaller or longer than the module borders.

In order to deal with the issue (1), we introduce a line selection algorithm, which filters out all the lines whose angular coefficient does not fall in certain intervals. In particular, we determine two sets of lines: $\hat{H}_t$, which contains all the horizontal lines, namely the ones whose slope is around zero (Fig. 1c):

$$\hat{H}_t = \left(\hat{h}_t^i, \quad i = 1 : \hat{H} | -\epsilon < m\left(\hat{h}_t^i\right) < +\epsilon\right), \tag{1}$$

being m the function for determining the angular coefficient of the line and ϵ a threshold chosen during the configuration setup.

At the same time, we determine the set of vertical lines $\hat{V}_t$, composed by the lines whose title angle is about $90^c irc$ (Fig. 1d):

$$\hat{V}_t = \left(\hat{v}_t^i, \quad i = 1 : \hat{V} | 90 - \epsilon < m\left(\hat{v}_t^i\right) < 90 + \epsilon\right). \tag{2}$$

Given $\hat{H}_t$ and $\hat{V}_t$, we solve the issues (2) and (3) by applying a line clustering algorithm. Fig. 1c, d point out the presence of multiple lines for each junction. We further refine both the sets $\hat{H}_t$ and $\hat{V}_t$ by computing the average slope m' and filtering out all the lines whose angular coefficient does not respect the condition $|m - m'| < \tau_m$. Then we apply a hierarchical clustering algorithm which fuses all the lines close together within a certain distance d_c. Consequently, the resulting sets H_t and V_t contain for each junction a single horizontal or vertical line respectively.

Then we compute the average horizontal lines tilt angle α, so as to perform a rotation of the image around its center and obtain the rotated frame $R_t = K_t \times F_t$ (Fig. 1e) with the following transformation matrix:

$$K_t = \begin{bmatrix} \cos\alpha & \sin\alpha & (1-\cos\alpha)\cdot x_0 - \sin\alpha \cdot y_0 \\ -\sin\alpha & \cos\alpha & \sin\alpha \cdot x_0 + (1-\cos\alpha)\cdot y_0 \end{bmatrix}. \tag{3}$$

Figure 1f, g show the results of the proposed line clustering algorithm; the horizontal and vertical lines have been rotated by using α and projected on R_t.

Finally, we apply our model of the panel to define the grid structure of the PV plant portion. It is based on three assumptions: (1) two vertical lines can be considered left and right module borders if their distance is comparable with the width W of a panel; (2) two horizontal lines can be considered top and down module borders if their distance is similar to the height H of a panel; (3) a PV module has exactly four vertices, namely two horizontal and two vertical borders. The application of such panel model to the sets H_t and V_t projected on R_t allows to detect the grid structure of the PV string. It is worth to mention that the proposed model-based technique also allows to correct the errors of the previous processing steps, since possible missing lines can be identified thanks to the PV plant model knowledge. Indeed, if the grid is not regular, namely the resulting PV string does not consist of adjacent consecutive panels, the proposed algorithm is able to add the missing lines and to detect the panel anyway.

The result of this step is a set of bounding boxes $B_t = (b_t^1, ..., b_t^{|B|})$ ($|B|$ is the number of PV panels detected at time t), which represent the locations of the PV modules in the image and, thus, the regions where local hot spot detection will be performed (Fig. 1h).

2.2 Local hot spot detection

The local hot spot detection algorithm identifies PV anomalies in a single frame, by applying specific heuristics in the regions delimited by the rectangles stored in the set B_t.

As anticipated, we observe that hot spots correspond to those regions in the panel with higher luminance, thus, instead than using absolute thresholds, in this paper we formulate the detection problem in terms of bi-dimensional local maxima search. Furthermore, the search procedure is not applied on the whole image, but instead only in the image region delimited by the borders of the PV module. To this aim, we adapt the water filling algorithm (Zhang et al. 2012). Such algorithm has been introduced in its original version for counting people in depth images, being the counting problem re-formulated in terms of local minima searching in depth images.

The idea of the water filling algorithm is graphically reproduced in Fig. 2; this algorithm is inspired by the natural process of puddles filling during a storm. Indeed, given an irregular surface, a raindrop falling will flow directly to the nearest cavity, due to gravity. Let's represent such situation

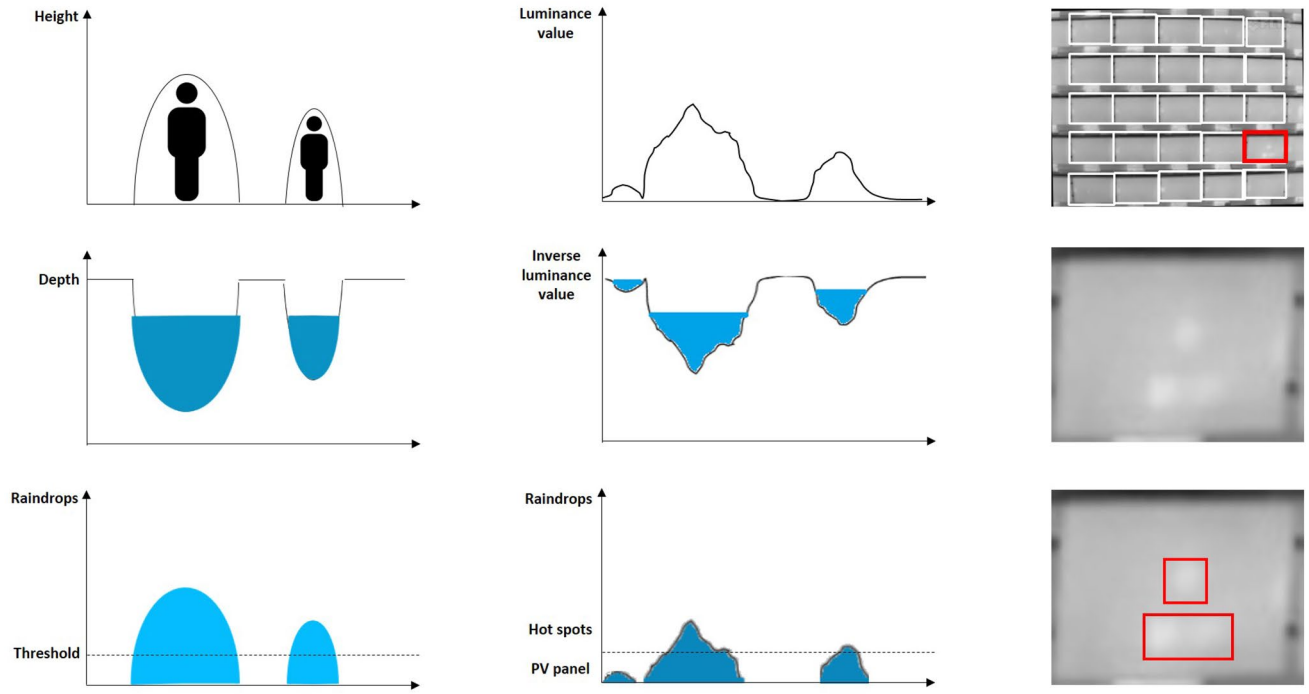

Fig. 2 Water filling for local hot spot detection. In the first column the algorithm, in its original form, detects the heads of the people by searching the local minima on the depth image (Zhang et al. 2012). In the second column, we detect the hot spots in a PV panel by searching the local minima on the inverse module image, since they correspond to local maxima in the original thermal image. In the third column, an example of PV panel with two hot spots correctly detected

on the ground with a gray scale image: each pixel intensity represent the height of the point; the highest intensity value (let's suppose 255) represent the ground layer; the holes on the ground corresponds to lower intensity values, in the range 0–254. Of course, the lower is the value, the deeper is the hole. Thus, finding the holes in the ground corresponds to searching for local minima in the image. In order to detect such holes, the water filling algorithm simulates a water drop and determine which are the regions with more water, since the greater is the depth of the holes, the greater is the amount of water needed to fill them.

Figure 2 (first column, on the left) shows this idea applied to the problem of people counting with depth images, as formulated by Zhang et al. (2012): the heads of the people captured by an overhead mounted depth sensor are definitely the parts of the body closest to the camera; since the depth sensor measures the distances of the pixels from the optic and represents them with gray scale intensity values, the heads can be detected by searching local minima regions in the depth image, namely the regions with the greater amount of raindrops.

Inspired by Zhang et al. (2012), we adapt the algorithm to our purposes and make it suited for addressing the problem of local hot spot detection. First of all, we transform the problem of local maxima search in a local minima search by considering the inverse values of the pixels in the thermal image. In this way, the hottest pixels will assume smaller gray scale intensity values. Then, we apply the water filling algorithm to detect hot spots.

In more details, let us define two sets of functions: the set $P_t^i(x, y)$ represents the luminance value of a generic pixel (x, y) belonging to the ith PV panel region delimited by the rectangle b_t^i; the set $G_t^i(x, y)$ counts, for each PV module, the number of raindrops in (x, y). For our purposes we will use the inverse luminance values, hereinafter indicated with $\overline{P_t^i}(x, y)$. Such function can be represented as a ground with holes and protuberances (see the second column of Fig. 2). The water filling algorithm is designed to simulate a rain fall, whose raindrops will move towards the cavities. To reproduce this effect, the method moves a raindrop from (x, y) to another point (x', y') in its neighbourhood until the following condition holds:

$$\overline{P_t^i}(x', y') + G_{t-1}^i(x', y') < \overline{P_t^i}(x, y) + G_{t-1}^i(x, y). \tag{4}$$

The seeds where the raindrop falls are chosen with a random procedure. After a finite number of iterations, a local minima (x_m, y_m) is found and the function $G_t^i(x_m, y_m)$ can be updated with a quantity δ of raindrops:

$$G_t^i(x_m, y_m) = G_{t-1}^i(x_m, y_m) + \delta. \tag{5}$$

After $N \times \delta$ raindrops the flood ends and the regions with a significant amount of water should be classified as hot spots. To this aim, we compute a binary image T_t^i whose generic pixel (x, y) of M_t^i is computed as follows:

$$T_t^i(x,y) = \begin{cases} 1 & \text{if } G_t^i(x,y) > \tau_H \\ 0 & \text{otherwise} \end{cases}. \tag{6}$$

In this way, the pixels with a number of raindrops greater than τ_H, namely the local minima, are white; so, the hot spots HS_t^i in the ith PV panel can be detected by searching the connected component labelling on T_t^i. Some examples are shown in the third column of Fig. 2. The quantity of raindrops in a shower δ, the number of showers N and the threshold τ_H are chosen by the human operator during the configuration set up.

If the panel junctions are particularly hot, it is not possible to distinguish them from real hot spots, since the luminance difference with respect to the background is big enough to detect such hot areas as local minima. Therefore, the only discriminant feature between hot junctions and hot spots is the position they occupy in the PV panel region. For this reason, our algorithm filters out from the set HS_t^i the rectangles that are too close to the PV module borders. Such final refinement allows to reduce significantly the number of false positives due to hot junctions.

2.3 Global hot spot detection

Local hot spot detection only exploits spatial information; the aim of global hot spot detection is to combine spatial information with temporal ones so as to increase the accuracy in the PV anomaly detection. It implies that all the occurrences of a given frame in the video are evaluated for taking the decision about the presence/absence of hot spot inside a given panel. Starting from this assumption, we introduce a tracking algorithm, with the aim to uniquely identify each panel, even if acquired by the camera frame by frame in different positions.

Since the precision of the currently available GPS sensors is not sufficient for tracking the PV panels, we propose the use of a multi-target tracking algorithm which takes into account the position of the PV panel in the image.

In more details, we perform a local data association inspired by our previous work (DiLascio et al. 2013). Let us define $P_t = (p_t^1, ..., p_t^{|P|})$ as the set of PV panels tracked at time t, being $|P|$ the number of PV panels tracked at time t. Thus, the position of the PV panel in the image is the only feature used in order to associate the jth module b_t^j detected at the current frame with the ith panel p_{t-1}^i tracked until the previous frame. So we apply a one-to-one overlap tracking algorithm, based on the computation of the similarity matrix S_t, where the generic element $s_t(i,j)$ represents the similarity between the b_t^j and p_{t-1}^i. The similarity is based on the euclidean distance d between the center of b_t^j and the center of p_{t-1}^i and it is computed for each pair (i, j) as follows:

$$s_t(i,j) = \begin{cases} 1 - \frac{d}{d_{max}} & \text{if } d \le d_{max} \\ 0 & \text{otherwise} \end{cases}, \tag{7}$$

being d_{max} the maximum displacement of the center of the PV panel between two consecutive frames.

Given S_t, the maximum value at the generic position (i_{max}, j_{max}) is computed and the association between $B_t^{i_{max}}$ and $P_{t-1}^{j_{max}}$ is performed, so that the information related to P_t^j is updated to the information available at the current frame. If a module can not be associated to any other previous PV panel, then a new identifier is created and the algorithm starts tracking this new module. Viceversa, in case a module can not be associated to any box, the module needs to be deleted. Anyway, two situations may arise: due to the movement of the drone, the module is no more present inside the scene; the module is still in the scene, but the corresponding box has not been detected due to an error during the detection step. Thus, in order to deal with such issues, we introduce the concept of *ghosts*; indeed, as in DiLascio et al. (2013), the module not associated is not immediately discarded and deleted from P_t, but instead is temporarily maintained. In case it does not appear again in g seconds (being g set in our experiments to 1 second), thus it will be discarded. Thanks to this choice, if a PV panel is not detected for a few frames due to detection errors, the algorithm is able to recover the identity of the module as soon as the abnormal situation is resolved. At the end of this step, all the PV panels tracked at time t are available in the set P_t.

P_t and HS_t are finally used so as to analyse the history of each PV module and then to perform global hot spot detection by a majority voting based approach. In more details, let us define N_{p_i} the total number of frames in which the module p_i has been visible and $N_{p_i}^{hs}$ the total number of frames in which the algorithm detected at least one hot spot in p_i. As soon as P_i is no more visible and, thus, is no more tracked, we verify the presence of an fault if the following condition holds:

$$\frac{N_{p_i}^{hs}}{N_{p_i}} > \tau_S. \tag{8}$$

The rationale behind this choice is that a PV panel is considered damaged if the hot spot is observed for a percentage of frames greater than τ_S, which regulates the sensitivity of anomaly detection. The lower is the value of this threshold,

Table 1 Description of the dataset used in our experiments

Name	Resolution	Panels	Local HS	Global HS
Video1	640 × 480	–	113	1
Video2	336 × 256	–	198	2
Video3	336 × 256	–	449	2
Video4	336 × 256	–	32	1
Video5	336 × 256	–	20	1
Video6	336 × 256	–	1048	8
Video7	336 × 256	–	1096	4
Video8	336 × 256	–	19	3
Video9	336 × 256	–	152	10
Video10	336 × 256	–	197	12
Video11	320 × 240	6123	126	4
Video12	320 × 240	2548	78	11
Video13	320 × 240	2064	97	15
Video14	320 × 240	2052	17	1
Video15	320 × 240	1428	12	1
Total		14,215	3654	76

the higher will be the hot spot detection sensitivity and the amount of possible false positives; vice versa, the greater is the value of τ_S, the higher will be the rejection of false positives to detriment of the recall.

3 Experimental results

In this section we will detail the experimental analysis we design for evaluating the proposed approach: in Sect. 3.1 the dataset used for our experimentation is introduced; Sect. 3.2 defines the indices used for performing a quantitative analysis, whose results are summarised in Sect. 3.3. Finally, a discussion about pros and cons of the proposed approach is presented in Sect. 3.4.

3.1 The dataset

The dataset used in our experimentation is summarized in Table 1, while some examples are provided in Fig. 3.[2]

The whole dataset consists of 15 videos, manually labelled by our experts with annotations for local hot spots (3, 654 panels images with hot spots) and global hot spot detection (76 different hot spots); we also provide the ground truths of a subset (from Video11 to Video15) for PV panel detection (14, 215 modules images). The images have been acquired with three different thermal cameras at resolutions 640 × 480, 336 × 256 and 320 × 240.

[2] The dataset, together with the annotations, is available for benchmarking purposes upon request at http://mivia.unisa.it.

In order to reproduce the several possible flight conditions, the flight plan of the UAV has not been designed for maximizing the performance; indeed, the human pilot has been free to move the drone over the PV plant in the way he considered more appropriate. As a result (see Fig. 3b, c, f or e, i, j), the UAV flies at different altitudes, so the PV panels have different sizes in the image plane; even if it is not evident in the figure, the altitude of the drone varies also during the same video, so making really hard the PV modules detection. Moreover, the flight routes have been completely variable and the PV plant has been inspected from West to East or from North to South and vice versa, so the modules have been captured with different orientations (Fig. 3m, n) and inclinations (Fig. 3o). The PV panels available in the dataset are also characterized by different real dimensions, color and disposition, since they belong to various real PV plants. The images have been acquired in different weather and illumination conditions, in order to include situations of shaded panel borders, low contrast between hot spots and module background and hot panel junctions, which are the most challenging aspects.

Note that a portion of the dataset, namely from Video1 to Video5, has been already used in our previous work (Arenella et al. 2017) for local hot spot detection, while all the other sequences have been proposed in this paper for the first time. According to our knowledge, we perform the biggest experimental analysis available in the literature up to now for PV anomaly detection.

3.2 Experimental protocol

The performance has been evaluated in terms of Precision (P), Recall (R) and F-Score (F):

$$P = \frac{TP}{TP + FP}, \tag{9}$$

$$R = \frac{TP}{TP + FN}, \tag{10}$$

$$F = 2 \cdot \frac{P \cdot R}{P + R}, \tag{11}$$

where TP, FP and FN represent, respectively, the number of True Positives (TP), False Positives (FP) and False Negatives (FN). The evaluation protocol classifies an event as true positive, false positive or false negative, differently for the three considered problems.

The ground truths for PV panel and local hot spot detection consist, frame by frame, of the image coordinates of the rectangles which surround the modules and the anomalies, respectively. Therefore, the true positives are computed by evaluating the overlap between the boxes associated to the object (panel or hot spot) at the ith frame, O_i, and the ground truth GT_i according to the Pascal Criterion (Everingham

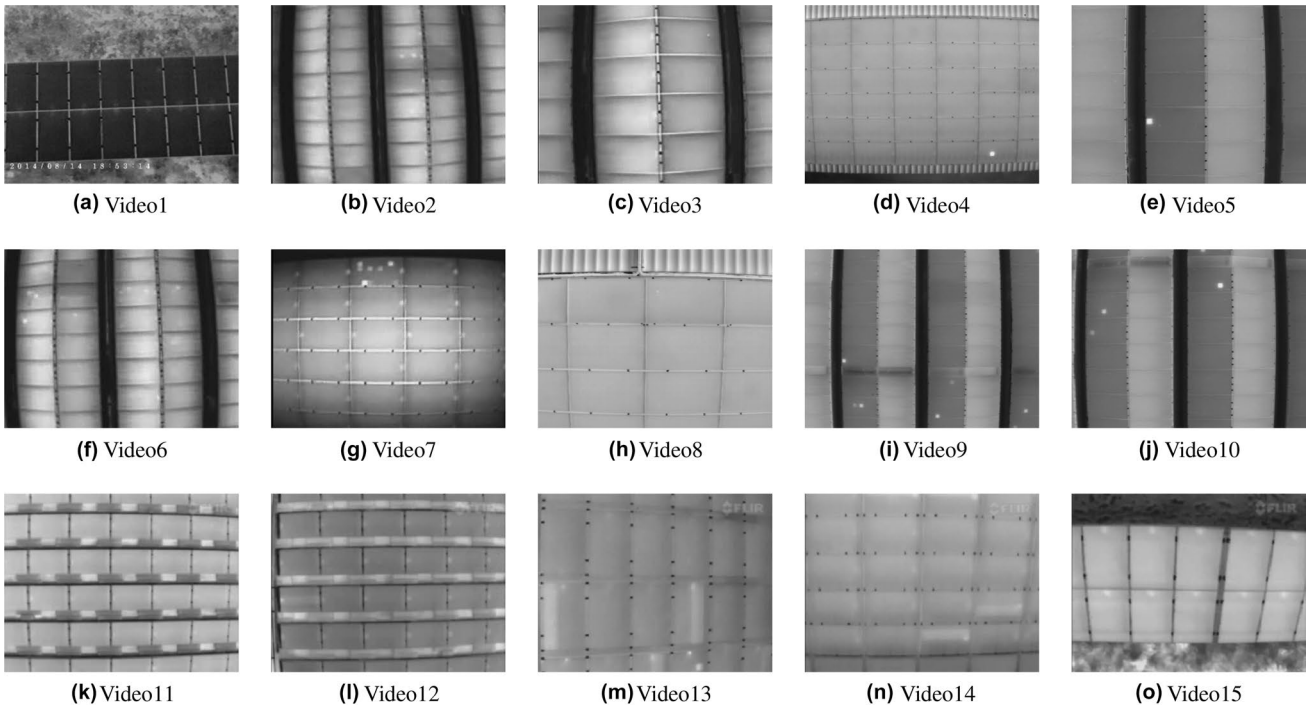

Fig. 3 Examples of images available in the dataset. The PV plants have been recorded with different thermal cameras and the UAV flies at various altitudes, so the modules have different sizes in the image plane. Moreover, the UAV flies over the PV plant following variable routes, thus the panels are captured with different orientations and inclinations

Table 2 Panel detection accuracy of the proposed method

Video	TP	FP	FN	P	R	F
Video11	6007	527	116	0.92	0.98	0.95
Video12	2452	344	96	0.87	0.96	0.92
Video13	1590	541	474	0.75	0.76	0.76
Video14	1568	781	484	0.66	0.76	0.71
Video15	1221	408	207	0.75	0.85	0.80
Total	12,838	2601	1377	0.83	0.90	0.87

et al. 2010). In more details, O_i is a true positive if the following condition is satisfied:

$$\frac{area(O_i \cap GT_i)}{area(O_i \cup GT_i)} \geq 0.4, \tag{12}$$

otherwise O_i can be considered a false positive. All the ground truth elements not associated to objects detected by the algorithm are considered false negatives. In this way, not only a miss or a false positive, but also bounding boxes that are not well centred around the target (panel or hot spot) are penalized.

The definition of TP, FP and FN for global hot spot detection is slightly different. Indeed, in this case the ground truth is not generated frame by frame, but instead panel by panel and contains the information related to the fact that a PV panel is (or is not) faulty. Thus, a TP corresponds to a panel containing an hot spot and identified as faulty by the proposed approach. Vice versa, a FP corresponds to a panel identified as faulty by the system but which does not contain any hot spot. Finally, a FN is associated to a missing, namely to a faulty panel which is not detected as damaged by the proposed approach.

3.3 Results

In the following, the results for each step, namely panel detection, local hot spot detection and global hot spot detection will be presented in Sects. 3.3.1, 3.3.2 and 3.3.3,

Table 3 Local hot spot detection accuracy of the proposed method

Video	TP	FP	FN	P	R	F
Video1	82	32	31	0.72	0.73	0.72
Video2	185	62	13	0.75	0.93	0.83
Video3	349	93	100	0.79	0.78	0.78
Video4	29	11	3	0.73	0.91	0.81
Video5	20	3	0	0.87	1.00	0.93
Video6	899	369	149	0.71	0.86	0.78
Video7	654	174	442	0.79	0.60	0.68
Video8	17	11	2	0.61	0.89	0.72
Video9	80	28	72	0.74	0.52	0.61
Video10	141	41	56	0.77	0.72	0.74
Video11	52	27	74	0.66	0.41	0.50
Video12	30	42	48	0.41	0.38	0.40
Video13	50	70	47	0.41	0.51	0.46
Video14	10	11	7	0.47	0.59	0.52
Video15	7	14	5	0.33	0.58	0.42
Total	2605	988	1049	0.73	0.71	0.72

Table 4 Performance comparison of the proposed method with a state of the art color-based approach for local hot spot detection

Method	Arenella et al. (2017)			Proposed method		
Video	P	R	F	P	R	F
Video1	0.42	0.58	0.49	0.72	0.73	0.72
Video2	0.45	0.90	0.61	0.75	0.93	0.83
Video3	0.51	0.69	0.59	0.79	0.78	0.78
Video4	0.78	0.78	0.78	0.73	0.91	0.81
Video5	0.59	0.85	0.69	0.87	1.00	0.93
Total	0.49	0.73	0.59	0.77	0.82	0.79

respectively. Finally, an analysis about the processing time is conducted in Sect. 3.3.4.

3.3.1 Panel detection accuracy

Table 2 reports the PV panel detection accuracy achieved by the proposed method on the 14, 215 images of modules. The Recall of the system is 0.90, so implying that 90% of the PV panels have been correctly detected and analysed for recognizing possible faults. The Precision and the F-Score, namely 0.83 and 0.87 respectively, confirm that the proposed algorithm for PV modules detection is able to find a good trade off between sensitivity and false positive rejection. The performance of the algorithm is very impressive on Video11 and Video12, where the panel contours are clear, the altitude and the speed of the drone are constant and the modules of the plant are installed on the ground, perpendicular with respect to the camera. The accuracy decreases when the previous conditions are not totally respected. In Video13 and especially in Video14 the module borders are very smooth and not easily visible even for humans, so making the task of the algorithm really challenging; in Video15 the UAV flies at different altitudes and speeds and the panels are inclined, so the dimensions of the modules in the image plane are variable and cause detection errors.

3.3.2 Local hot spot detection accuracy

Table 3 reports the local hot spot detection accuracy achieved by the proposed method on 3, 654 images of hot spots. The Recall of the algorithm is 0.71. It means that 71% of the PV anomalies have been correctly detected. Furthermore, the F-Score of 0.72 is a clear insight of the balancing of the algorithm between sensitivity and false positives rejection.

The effectiveness of the proposed method is further confirmed by the comparison of the results with the approach proposed in Arenella et al. (2017), reported in Table 4. Since such method has been tested only on a portion of our dataset, the performance comparison has been limited to such videos. Our method significantly outperforms the one proposed in Arenella et al. (2017) over all the performance indices, so demonstrating our hypothesis that local maxima search with water filling is more accurate than

Table 5 Global hot spot detection accuracy of the proposed method

Video	TP	FP	FN	P	R	F
Video1	1	0	0	1.00	1.00	1.00
Video2	2	0	0	1.00	1.00	1.00
Video3	2	0	0	1.00	1.00	1.00
Video4	1	0	0	1.00	1.00	1.00
Video5	1	0	0	1.00	1.00	1.00
Video6	6	0	2	1.00	0.75	0.86
Video7	4	0	0	1.00	1.00	1.00
Video8	2	3	1	0.40	0.67	0.50
Video9	7	0	3	1.00	0.70	0.82
Video10	12	4	0	0.75	1.00	0.86
Video11	3	2	1	0.60	0.75	0.66
Video12	5	4	6	0.55	0.45	0.50
Video13	8	2	7	0.80	0.53	0.63
Video14	1	1	0	0.50	1.00	0.66
Video15	1	0	0	1.00	1.00	1.00
Total	56	14	20	0.80	0.74	0.77

a color-based approach for hot spot detection. Note that there are not any other methods available in the literature whose results have been computed over available datasets or whose code is publicly available. This is why our comparison has been limited to Arenella et al. (2017).

3.3.3 Global hot spot detection accuracy

Table 5 reports the global hot spot detection accuracy achieved by the proposed method on 76 panels with hot spots. Since the algorithm has been able to correctly recognize 56 over 76 faulty modules, about 3 anomalies on 4 have been globally detected (the Recall is 0.74, while for local hot spot detection it was 0.71). The Precision of 0.80 and the F-Score of 0.77 allow to conclude that: (1) the global hot spot detection is able to improve the accuracy of the local one by considering all the performance indices; (2) the balancing values of Precision and Recall confirm the capability of the algorithm to find a good trade-off between sensitivity and false positives rejection.

3.3.4 Processing time analysis

To analyse the efficiency of the proposed method, we perform an experimental evaluation of the processing time required by the proposed algorithm on an Intel Joule 570X Board, which has a CPU Intel Atom TS700 (1.7–2.4 GHz) and 4 GB of RAM LPDDR4. Such device is a System on a Module (SoM), so it can be installed on the UAV to carry out real-time PV inspection during the flight.

Since our dataset consists of videos captured at different resolutions, we have been able to notice that the proposed algorithm processes about 7 frames per seconds in case of 640×480 resolution images and from 8 to 11 frames per second (fps) at resolutions 336×256 and 320×240. As we expect, the most burdensome step is the PV panel detection, which requires about 75% of the total processing time especially due to the use of the Hough transform. Almost all the remaining time is spent for local hot spot detection.

In any case, the processing speed of the proposed algorithm is suited for real-time PV inspection during the flight using a SoM equipped by the UAV.

3.4 Discussion

The experimental results demonstrate the effectiveness of the proposed method for automatic PV inspection and pose the basis for future investigations in this field. Indeed, various insights emerge from the analysis performed on our dataset.

The proposed method achieves a Recall of 90% for PV panel detection, since it correctly detects 12,838 over 14,215 considered modules. It is therefore able to successfully deal with shaded panel contours, adverse weather and illumination conditions and sudden UAV movements. Although the performance is really remarkable considering the challenging task, it means that 10% of the PV modules have not been inspected to check for thermal anomalies. Such information gives a quantitative idea of the reliability of automatic PV inspection with UAVs. It is definitely true that this technique can be profitably used for its economic benefits but it is also important to consider that the fault diagnosis report may be not complete.

We demonstrate the superiority of our local hot spot detection method with respect to a state of the art color-based approach (Arenella et al. 2017). It means that our

algorithm, which performs a local maxima search in the panel region instead of applying static color threshold, is at the same time more sensitive for anomaly detection (Recall 0.82 vs 0.73) and more precise in false positives rejection (Precision 0.77 vs 0.49). Despite the proved effectiveness with respect to another state of the art approach, the overall local hot spot detection Recall of the proposed method is 0.71, so the algorithm is able to detect 71% of the visible anomalies. The global hot spot detection algorithm is able to improve the performance, achieving a Recall of 0.74 and a Precision of 0.80, so confirming the validity of the proposed multi-frame tracking. Such result, in addition to giving us other insights on the reliability level of the fault detection system, allows us to make further observations on the causes of these errors.

Indeed, it is important to remind that a portion of the error is due to hot panel junctions, whose correct exclusion strongly depends on the precision of the bounding box which surrounds the PV module and, thus, on panel detection accuracy; local hot spot detection errors can be due to hot junctions not excluded and wrongly recognized as anomalies or hot spots excluded because incorrectly considered junctions. This is one of the reasons why we decided to use the Pascal Criterion for determining TP, FP and FN for panel detection, since the use of both intersection and union between the bounding boxes should assure that the modules correctly detected have also a rectangle well centred on the panel. Further improvements on the PV panel detection algorithm would have a positive impact not only on the performance of the respective step, but also on the subsequent anomaly detection steps.

Another relevant cause of error is definitely the tracking algorithm based only on image information (reminding that the panel are almost equal in terms of color and shape, and the position becomes the only discriminant feature), since the geographic coordinates collected with the currently available GPS sensors are not sufficiently accurate. The research of more accurate geo-localization systems is surely a future direction that should be investigated for improving the quality of automatic PV inspections with UAVs.

Finally, we demonstrate that the proposed approach is able to run in real-time over a SoM equipped by the UAV, so it would be possible to perform the analysis during the flight.

4 Conclusions

In this paper we propose a novel method for real-time thermographic inspection of photovoltaic plants with UAVs.

The proposed approach is able to detect PV panels by extracting the structural features of the plant without using color information and dealing successfully with troubles like shaded panel contours, variable weather and illumination conditions, UAV vibrations and thermal irregularities. We demonstrate that our novel approach for local hot spot detection, formulated in terms of searching of local maxima in the PV panel region, outperforms a state of the art method based on color features and static thresholds. The global hot spot detection technique is able to further improve the local hot spot detection accuracy, by using a multi-frame panel tracking algorithm which allows to take the final decision about the possible fault by considering the complete history of the hot spot in the video.

The quantitative performance evaluation, carried out on a very wide dataset which we annotated with labels for PV panel, local hot spot and global hot spot detection and made available upon request, demonstrate the effectiveness of the proposed method for the problem at hand and give interesting insights for future research directions.

Acknowledgements This research has been partially supported by A.I. Tech s.r.l. (http://www.aitech.vision). We would like to thank Topview s.r.l. (http://www.topview.it) for providing the videos used in our experimentation.

References

Addabbo P, Angrisano A, Bernardi ML, Gagliarde G, Mennella A, Nisi M, Ullo S (2017) A UAV infrared measurement approach for defect detection in photovoltaic plants. In: IEEE international workshop on metroaerospace, pp 345–350

Aghaei M, Bellezza Quater P, Grimaccia F, Leva S, Mussetta M (2014) Unmanned aerial vehicles in photovoltaic systems monitoring applications. In: European photovoltaic solar energy 29th conference and exhibition, pp 2734–2739

Aghaei M, Gandelli A, Grimaccia F, Leva S, Zich R (2015a) IR real-time analyses for PV system monitoring by digital image processing techniques. In: IEEE international conference on event-based control, communication, and signal processing (EBCCSP), pp 1–6

Aghaei M, Grimaccia F, Gonano CA, Leva S (2015b) Innovative automated control system for PV fields inspection and remote control. IEEE Trans Ind Electron 62(11):7287–7296

Aghaei M, Dolara A, Leva S, Grimaccia F (2016a) Image resolution and defects detection in PV inspection by unmanned technologies. In: IEEE power and energy society general meeting (PESGM), pp 1–5

Aghaei M, Leva S, Grimaccia F (2016b) PV power plant inspection by image mosaicing techniques for IR real-time images. In: IEEE photovoltaic specialists conference (PVSC), pp 3100–3105

Arenella A, Greco A, Saggese A, Vento M (2017) Real time fault detection in photovoltaic cells by cameras on drones. In: Springer international conference on image analysis and recognition (ICIAR), pp 617–625

Buerhop C, Scheuerpflug H (2014) Field inspection of PV-modules using aerial, drone-mounted thermography. In: EU-PVSEC

Buerhop C, Schlegel D, Niess M, Vodermayer C, Weißmann R, Brabec C (2012a) Reliability of IR-imaging of PV-plants under operating conditions. Elsevier Sol Energy Mater Sol Cells 107:154–164

Buerhop C, Weißmann R, Scheuerpflug H, Auer R, Brabec C (2012b) Quality control of pv-modules in the field using a

remote-controlled drone with an infrared camera. In: European photovoltaic solar energy conference and exhibition
Carletti V, Greco A, Saggese A, Vento M (2018) Multi-object tracking by flying cameras based on a forward–backward interaction. IEEE Access 6:43905–43919
DiLascio R, Foggia P, Percannella G, Saggese A, Vento M (2013) A real time algorithm for people tracking using contextual reasoning. Comput Vis Image Underst 117(8):892–908
Djordjevic S, Parlevliet D, Jennings P (2014) Detectable faults on recently installed solar modules in western australia. Elsevier Renew Energy 67:215–221
Dotenco S, Dalsass M, Winkler L, Würzner T, Brabec C, Maier A, Gallwitz F (2016) Automatic detection and analysis of photovoltaic modules in aerial infrared imagery. In: IEEE international conference on applications of computer vision (WACV), pp 1–9
Everingham M, Van Gool L, Williams CK, Winn J, Zisserman A (2010) The pascal visual object classes (VOC) challenge. Springer Int J Comput Vis 88(2):303–338
Goutte C, Gaussier E (2005) A probabilistic interpretation of precision, recall and F-score, with implication for evaluation. In: Springer European conference on information retrieval, pp 345–359
Grimaccia F, Aghaei M, Mussetta M, Leva S, Quater PB (2015) Planning for PV plant performance monitoring by means of unmanned aerial systems (UAS). Springer Int J Energy Environ Eng 6(1):47–54
Grimaccia F, Leva S, Dolara A, Aghaei M (2017a) Survey on PV modules common faults after an o&m flight extensive campaign over different plants in italy. IEEE J Photovolt 7(3):810–816
Grimaccia F, Leva S, Niccolai A (2017b) PV plant digital mapping for modules defects detection by unmanned aerial vehicles. IET Renew Power Gener 11(10):1221–1228
Guerriero P, Daliento S (2017) Automatic edge identification for accurate analysis of thermographic images of solar panels. In: IEEE international conference on clean electrical power (ICCEP), pp 768–772
Hu Y, Cao W, Ma J, Finney SJ, Li D (2014a) Identifying PV module mismatch faults by a thermography-based temperature distribution analysis. IEEE Trans Device Mater Reliab 14(4):951–960
Hu Y, Cao W, Wu J, Ji B, Holliday D (2014b) Thermography-based virtual MPPT scheme for improving PV energy efficiency under partial shading conditions. IEEE Trans Power Electron 29(11):5667–5672
Jiang L, Su J, Li X (2016) Hot spots detection of operating PV arrays through IR thermal image using method based on curve fitting of gray histogram. In: MATEC web of conferences, vol 61, p 06017
Leva S, Aghaei M, Grimaccia F (2015) Pv power plant inspection by UAS: correlation between altitude and detection of defects on PV modules. In: IEEE international conference on environment and electrical engineering (EEEIC), pp 1921–1926
Li X, Hu W, Shen C, Zhang Z, Dick A, Hengel AVD (2013) A survey of appearance models in visual object tracking. ACM Trans Intell Syst Technol 4(4):58
Quater PB, Grimaccia F, Leva S, Mussetta M, Aghaei M (2014) Light unmanned aerial vehicles (UAVS) for cooperative inspection of pv plants. IEEE J Photovolt 4(4):1107–1113
Tsanakas JA, Chrysostomou D, Botsaris P, Gasteratos A (2015) Fault diagnosis of photovoltaic modules through image processing and canny edge detection on field thermographic measurements. Int J Sustain Energy 34(6):351–372
Tsanakas JA, Ha L, Buerhop C (2016) Faults and infrared thermographic diagnosis in operating C–Si photovoltaic modules: a review of research and future challenges. Elsevier Renew Sustain Energy Rev 62:695–709
Tsanakas JA, Ha LD, Al Shakarchi F (2017) Advanced inspection of photovoltaic installations by aerial triangulation and terrestrial georeferencing of thermal/visual imagery. Elsevier Renew Energy 102:224–233
Yilmaz A, Javed O, Shah M (2006) Object tracking: a survey. ACM Comput Surv 38(4):13
Zhang X, Yan J, Feng S, Lei Z, Yi D, Li SZ (2012) Water filling: unsupervised people counting via vertical kinect sensor. In: IEEE international conference on advanced video and signal-based surveillance (AVSS), pp 215–220